Scilight

Photochemistry and Spectroscopy

https://www.sciltp.com/journals/ps

Article

Optical Characterization of 3D Bio-Hybrid Actuators

Andrea Pianetti [1,†], Ilaria Venturino [1,2,†], Giulia Simoncini [1,2], Samim Sardar [1,3], Ludovico Aloisio [1,2], Paola Moretti [4], Giuseppe Maria Paternò [1,2], Chiara Bertarelli [4], Cosimo D'Andrea [1,2,*] and Guglielmo Lanzani [1,2,*]

[1] Center for Nanoscience and Technology, Istituto Italiano di Tecnologia, Via Rubattino 81, 20134 Milano, Italy
[2] Department of Physics, Politecnico di Milano, Piazza Leonardo da Vinci 32, 20133 Milano, Italy
[3] Department of Chemistry, National Institute of Technology Warangal, Telangana 506004, India
[4] Dipartimento di Chimica, Materiali e Ingegneria Chimica "Giulio Natta", Politecnico di Milano, Piazza Leonardo da Vinci 32, 20133 Milano, Italy
* Correspondence: cosimo.dandrea@polimi.it (C.D.); guglielmo.lanzani@polimi.it (G.L.)
† These authors contributed equally to this work.

How To Cite: Pianetti, A.; Venturino, I.; Simoncini, G.; et al. Optical Characterization of 3D Bio-Hybrid Actuators. *Photochemistry and Spectroscopy* **2026**, *2*(1), 4. https://doi.org/10.53941/ps.2026.100004

Received: 31 October 2025
Revised: 28 November 2025
Accepted: 3 December 2025
Published: 28 January 2026

Abstract: Bio-hybrid actuators (BHAs) integrate biological components, such as skeletal muscle cells, with synthetic materials to generate motion through external stimuli. Here, we study the use of light to remotely control 3D bio-hybrid actuators. Specifically, the employment of the amphiphilic azobenzene derivative Ziapin2 to modulate cell membrane capacitance and induce contraction has been proved to be effective for myotube in 2D planar substrates. Transitioning from 2D planar substrates to 3D scaffolds demands the full characterization of the interaction of light with the cell seeded scaffold. Scattering analysis, confocal microscopy, and time-resolved photoluminescence (TRPL) have been effectively used to investigate and model light interaction of these 3D structures. The application of these techniques allowed us to optimize sample preparation and quantitative study the behavior, in a non-destructive way, on this new class of biomaterials. This study aims at establishing a foundation for the characterization of scalable, optically controlled 3D bio-hybrid actuators with applications in soft robotics and implantable biomedical device.

Keywords: bio-hybrid actuators; biorobotics; biomaterials; optical spectroscopy; molecular phototransducers

1. Introduction

Biohybrid actuators represent a rapidly growing field at the intersection of biology, engineering, and materials science [1]. These systems, which integrate biological components such as cells or tissues with synthetic materials, have gained attention due to their potential applications in soft robotics, medical devices, and tissue engineering [2–4]. Biohybrid robots (biobots), inspired by natural organisms, are designed to possess capabilities that traditional synthetic actuators struggle to achieve, such as adaptive movement, self-healing, and energy-efficient operation [5,6]. In the medical field, biohybrid actuators can pave the way for advanced prosthetics and assistive devices, while in tissue engineering, they can facilitate the development of functional bioengineered constructs for regenerative medicine [7]. Among the various design strategies, three-dimensional (3D) architectures are promising, as they allow for more complex and biomimetic structures, enhancing the functionality and efficiency of biohybrid systems, although they are more difficult to realize [8].

One of the critical aspects in designing biohybrid actuators is the selection of activation methods. Electrical stimulation has been widely employed due to its ability to precisely control contractile tissues, however it comes with significant drawbacks, including inflammatory responses, limited spatial control, and the requirement for

invasive wiring [9]. Light-based activation, in contrast, offers a non-contact, highly controllable, and spatially precise alternative [10,11].

So far, Ziapin2, a chemically synthetized amphiphilic azobenzene that integrates in cell's membrane, has been proven to modulate cells' membrane potential with light stimulus in different cells 'lines [12–15]. Specifically, in 2D myotubes structures, triggering of muscular cells contractions was achieved upon blue light stimulation [13]. The cellular response results from a cascade of events initially triggered by an optomechanical effect that alters the cell's membrane thickness [12]. This change activates strain-sensitive ion channels, leading to the generation of an action potential [16]. The success of Ziapin2 highlights its potential for application in more complex 3D bioactuators. However, the transition from 2D to 3D geometries presents several challenges, including limited light penetration and increased scattering or parasitic losses [17].

In this work, we fabricate hydrogel scaffolds via 3D bioprinting and seed them with C2C12 skeletal muscle cells prior to introducing Ziapin2 as a phototransducer. We then apply a range of optical characterization techniques to evaluate whether our construct is suitable for light-driven actuation. Specifically, we investigate the scattering and absorption properties of the hydrogel, as these features influence light penetration and energy distribution. Additionally, we examine how Ziapin2 interacts with the hydrogel itself as well as with embedded cells. By analyzing these interactions, we aim to establish the feasibility of our material for light-based biohybrid actuation, paving the way for future advancements in the field. As a result, the 3D printed scaffolds treated with Ziapin2 were effectively able to contract upon visible light stimulation, proving that non-genetic optostimulation can be applied efficiently to drive collective motion in complex and highly scattering 3D biohybrid constructs.

2. Materials and Methods

2.1. Cell Culture and Differentiation

C2C12 cells (ATCC) were cultured at 37 °C and 5% CO_2. Cells were kept under 70% of confluence to avoid damage and they were passed no more than 15 times. The maintenance medium contained Dulbecco's modified Eagle's medium (DMEM) supplemented with Fetal Bovine Serum (10%), Glutamine (2%), Penicillin-Streptomycin (1%). The differentiation medium contained Dulbecco's modified Eagle's medium (DMEM) supplemented with Horse Serum (10%), Glutamine (2%), Penicillin-Streptomycin (1%).

2.2. 3D Sample Fabrication

The 3D geometry was achieved using a 3D printing approach with a printer supplied by CELLINK. This printer is specifically designed for printing hydrogel or polymer in combination with cells and it incorporates an appropriate filter to ensure the sterility required for the printing process. The ink called GELXA LAMININK 121 was used as matrix. The full process is reported in Figure 1. The first step of the fabrication process was warming up the hydrogel for 20–30 min inside an incubator to increase its fluidity and facilitate cellular encapsulation. The ink is then transferred to a 5 mL syringe (Figure 1A). To encapsulate the cells inside the hydrogel, they need to be detached from their flask and, after the centrifugation process, resuspended in the appropriate amount of medium. The appropriate ratio between hydrogel and cells is 10 µL of cells per mL of hydrogel. The cells suspended in the medium are aspirated using a syringe. The two syringes are connected through a Luer-lock adapter, and the cells are mixed with the hydrogel (See Figure S1). At this stage of the procedure, it is important to ensure proper mixing of the cells while avoiding air bubble incorporation. To ensure that the cells can fully colonize the hydrogel during their growth, their concentration should be at least 800,000 cells per mL of hydrogel. The syringe containing the cells and the ink is placed inside the printer with a G22 nozzle (Figure 1B). The printing speed was set to 5 mm/s; a higher speed produces thicker lines, but printability is reduced. The syringe was kept at a temperature of 23 °C, whereas the printer bed was set at 15 °C. The working pressure, needed to eject the ink outside the nozzle, was set to 20 kPa. We obtained a 15 × 1.5 × 0.5 mm^3 cylinder, as depicted in Figure 1C. The polymerization of the hydrogel was obtained through 20–30 s of UV light (365 nm). This step is necessary to ensure that the hydrogel remains structured during cellular growth. After printing, the 3D samples were covered with the maintenance medium and placed inside the incubator. The same procedure, excluding cellular encapsulation, was performed using only the ink, in order to compare the material with the biomaterial throughout the experiments. Approximately four days after printing, the medium was switched to the differentiation medium and changed every two days. The maturation process takes time, so we decided to conduct all experiments 15 days after seeding. The samples without biological material underwent the same medium changes to ensure consistent treatment across both sample types. Indeed, due to its biocompatibility and long-term degradability, the hydrogel may have undergone changes over the 15-day period and with frequent medium exchanges.

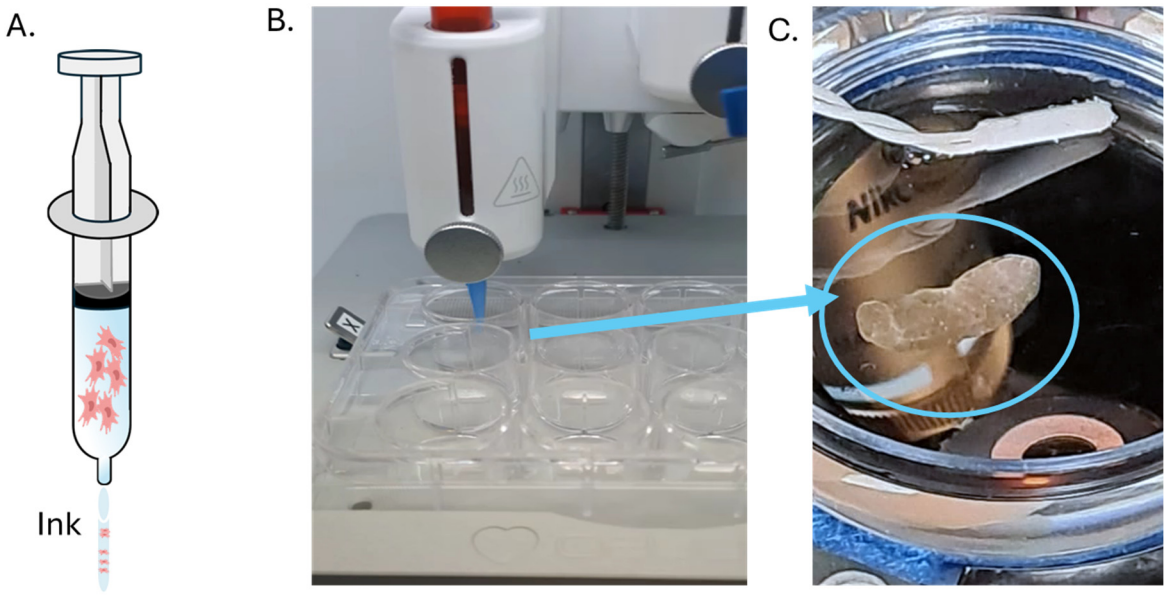

Figure 1. (**A**) Preparation of the bio-ink; (**B**) The printing process in the multiwell; (**C**) A close look of the printed 3D scaffold.

2.3. Ziapin2 Uptake

The 3D structures, both with and without cells, were treated with Ziapin2. The molecule was initially dissolved in DMSO at a concentration of 2 mM and then diluted in fresh differentiation medium to obtain four final concentrations: 10 µM, 25 µM, 50 µM, and 100 µM. The 25 µM concentration had already been used in planar conformation, with an incubation time of 10 min. Here, since 3D structures are more difficult to penetrate, the incubation time was extended to 1 h [13].

2.4. Optical Characterization

Optical Measurements have been carried out both within the sole hydrogel and the hydrogel-cell matrix. To evaluate absorption and scattering and to calculate the haze factor, a Spectrophotometer combined with an integrating sphere was used. The spectrophotometer is a Perkin Elmer Lambda, equipped with tungsten lamps (320–3300 nm), a monochromator and a photomultiplier with the spectral range 180–860 nm. A custom 3D-printed mask was designed to hold the gels at the entrance of the integrating sphere. A control measurement was performed using the empty mask and glass system, which was used as a reference for the measurements with the gels in place.

2.5. Optical Mask

The hydrogel, both with and without cells, needs to be placed inside a custom-made chamber to ensure the stability of the structure during the optical characterization. The mask was designed using Blender software and then printed using an Ultimeker S5 3D printer. The mask was made of polylactic acid (PLA) and was designed to have an internal chamber of 2 × 10 mm^2. The image of the chamber is reported in Figure S2.

2.6. Fluorescent Analysis

To support the time-resolved photoluminescence (TRPL) measurements and optical characterization, fluorescence imaging was performed. These images were captured using an inverted confocal laser microscope, the Nikon Eclipse Ti2. The software used for acquisition was NIS-Elements, Nikon Imaging Software. The objective used was 20×.To visualize the cells inside the hydrogel, they were treated with Hoechst, which stained the cell nuclei. It was diluted to a final concentration of 1:500 and incubated simultaneously with Ziapin2.

2.7. Contraction Video

The videos of the contraction of the 3D structures were obtained using a Nikon Eclipse Ti-S inverted microscope, coupled with a cyan LED (470 nm) source by Lumencor. The objectives used were 20×/0.50NA and 4×/0.13NA, both purchased from Nikon Instruments Italia (Campi Bisenzio, Italy). The videos were collected using PVCam software (version 3.10.1.1). The cells were stimulated with a series of light pulses at a frequency of

1 Hz. Each light pulse was 200 ms long. The power density used was 42 mW/mm^2 with a 20× objective and 5 mW/mm^2 with a 4× objective.

2.8. Contraction Video Analysis

The recorder time lapse was first reconstructed using Fiji software and subsequently processed with a Matlab script. The script employs a visual tracking algorithm that monitors the motion of a selected object across all video frames. The algorithm partitions the chosen region of interest (ROI) into smaller subregions and computes the coordinates of each one. These coordinates are compiled into a matrix containing the position of each point. Because all recordings begin from a resting state, this initial frame is defined as the zero reference for the system, enabling calculation of the average displacement of each point from its starting position. The mean distance for the ROI is obtained by averaging the displacements of all points within it. This approach was used to extract the average contraction trajectory of the myotubes [13].

2.9. Time Resolved Photoluminescence

Time-Resolved Photoluminescence (TRPL) measurements were carried out to assess Ziapin2's photoluminescence evolution in time up to 100 ps after laser excitation at 470 nm to evaluate its fast dynamic response. TRPL experiments were carried out using a femtosecond laser source coupled to a streak camera detection system (Hamamatsu C5680). A Ti:sapphire laser (Coherent Chameleon Ultra II, pulse bandwidth of about 140 fs, repetition rate of 80 MHz, and maximum pulse energy of 50 nJ) was used to pump a second- harmonic crystal (β-barium borate) to tune the pump wavelength to 470 nm. The sample has been mounted in a home-made microscope with a 20× objective. The measurements here shown were performed recording the first 130 ps of the temporal decay, with a temporal Instrumental Response Function (IRF) of 2.7 ps.

3. Results

3.1. Scattering of 3D Hydrogel Scaffolds

The 3D-printed GelMA structure enhanced cellular organization and force output. However, the compound is not entirely transparent to light due to both the material's intrinsic properties and the presence of myotubes within it. Before implementing optical stimulation, it is crucial to first examine how the hydrogel alone interacts with light and whether the biological component alters this interaction.

We characterized the scattering properties of the hydrogel structure by performing both spatial and temporal measurements. In the first case an integrating sphere has been use to calculate the haze factor which depends on the angular redistribution of incident light as it interacts with the material, affecting light penetration and diffusion. Temporal measurements, on the other hand, refer to the multiple scattering events estimation by measuring the broadening of an ultrashort light pulses propagating inside the medium.

Spatial scattering measurements were conducted using a spectrophotometer coupled with an integrating sphere, which enables the precise quantification of the haze factor. The haze factor is defined as the ratio of diffusely transmitted light to total transmitted light, providing a measure of how much light is scattered at wide angles rather than passing directly through the material. This measurement is performed using a standard geometry, where a collimated light beam is directed perpendicularly onto the sample. In our case, we built a homemade mask to keep the hydrogel perpendicular to the incident beam.

The integrating sphere collects both the total transmitted light and the scattered light, distinguishing between direct and diffused transmission. A high haze value, higher than 50% indicates opaqueness and strong light diffusion, while a low haze value means high transparency and low diffusion. This analysis allows us to optimize the trade-off between light penetration depth and efficient excitation of Ziapin2 within the 3D hydrogel. The data in Figure 2A show that both gel samples, with and without cells, exhibited a high haze factor (around 75%), consistent with the material's opaque appearance. This indicates that the presence of cells does not significantly alter the light interaction of the overall system, which is primarily determined by the printed gel. Having a high haze can result in two antagonistic effects on light propagation in the case of our actuators: (1) it can enhance internal light scattering and distribution, allowing photons to interact more by increasing the possibilities of reaching the target (2) It can imply that light is being predominantly confined to the outer layers. This is due to the reduced photon penetration depth—not primarily caused by absorption, but by extensive scattering, which redirects photons away from their original propagation path and limits their ability to reach deeper regions.

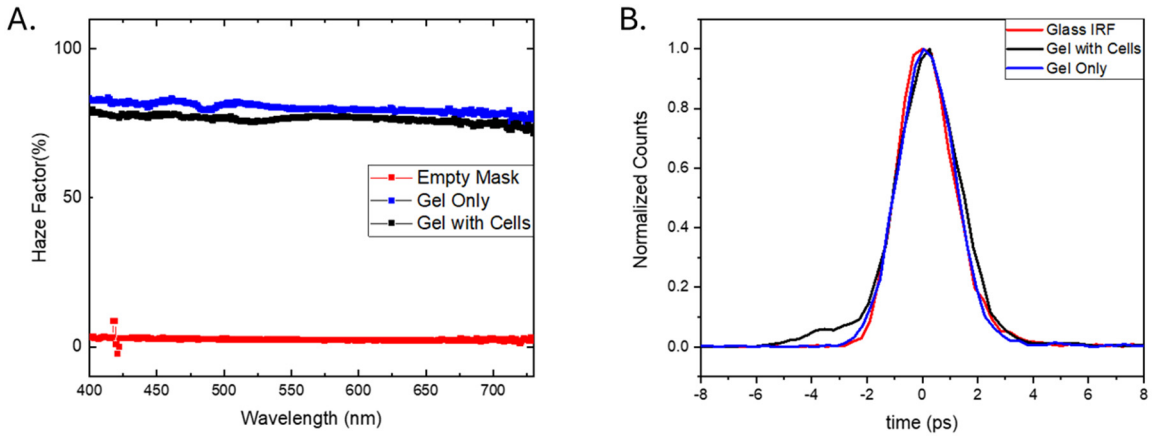

Figure 2. (**A**) Spatial Scattering results to calculate Haze factor of different samples (**B**) Pulse broadening for the different samples.

In order to assess multiple scattering properties of the sample we carried out temporal measurements by employing a pulsed laser source in combination with a streak camera detection system. A short laser pulse (~140 fs pulse width) was injected into the hydrogel, and the temporal broadening of the light exiting the sample was recorded to analyze photon pathlenghts distribution. In particular this technique enables direct measurement of pulse broadening as light travels through the sample, providing insight into the extent of multiple scattering events.

The data in Figure 2B show no substantial difference between gel samples (with or without cells) and the IRF reference (empty holder), indicating that the pulse traveling through the gels is not significantly broadened. In particular both the leading edge (ballistic and quasi-ballistic photons) and diffuse tail of the exiting pulse are not significantly distorted by the presence of the gel. This implies that multiple scattering is limited in our hydrogel because non significant pathlengtjhs distribution can be observed above the IRF of about 3 ps. Further analysis and/or simulations are needed to establish the possible effect of multiple scattering below the present IRF. Hence, optical scattering analysis thus reveals that light propagates through the hydrogel without significant temporal distortion despite the high haze, ensuring enough bulk excitation of embedded Ziapin2-sensitized cells.

3.2. Photophysics of Ziapin2 in the 3D Scaffolds

Once we confirmed that the scaffold's optical performance is consistent with the proposed application, we proceeded to investigate the stimulation process mediated by Ziapin2. Qualitative confocal measurements and quantitative TRPL measurements were subsequently performed to fully characterize the photoexcitation phenomena. As before, both the hydrogel alone and hydrogel with the cells were examined.

In Figure 3, we reported some relevant images of cells within the gel, acquired with confocal microscope. We used this technique for two purposes: i. to confirm the effective growth of cells inside the gel; ii. to monitor their morphology as myotubes. The results reported in Figure 3 showed how the myotubes had effectively colonized the volume of the scaffold, but staying inside and not overflowing the printed gel. Second, it was used to visualize Ziapin2: highlighted in green, it follows the myotube membrane rather than diffusing indiscriminately within the hydrogel. The figures report the images obtained for two different concentrations 25 and 50 μM, respectively.

Confocal imaging, based on measuring photoluminescence (PL) intensity of Ziapin2, is an ideal tool to evaluate molecules distribution, however, does not disclose the photophysics of the molecule, which is linked to its ability to photoisomerize and exert its photostimulation ability. Furthermore, confocal microscopy does not allow extracting information related to local concentration, especially when comparing different samples (i.e., the gel without cell has no specific spatial feature to image, being the molecule just distributed in the hydrogel so it makes it almost impossible to carry a side-by-side characterization with gel with cells). Thus, to gather more quantitative knowledge of such complex system, we measured TRPL of Ziapin2 by exciting it with a 475 nm pulsed laser coupled with a home-made microscope to investigate both time and space resolved PL.

The photophysical behavior of Ziapin2 is known to vary depending on the surrounding environment. In aqueous systems, Ziapin2 tends to aggregate, and its isomerization is suppressed, leading to a longer photoluminescence (PL) lifetime. In lipid membranes, by contrast, Ziapin2 regains conformational mobility and undergoes photoisomerization from the trans to the cis form. As a result, TRPL decay follows a well pronounced double-exponential profile: a short-lived component corresponding to the formation of the cis isomer, followed by a longer-lived component attributed to emission from the cis conformer. Based on these spectroscopic fingerprints,

measuring the TRPL of Ziapin2 within the gel provides insights into its behavior and, consequently, its local chemical environment. As reported in Figure 4, TRPL signals were recorded at two different depths within the 3D scaffold: (i) at the surface and (ii) approximately 200 µm inside the gel, where cells predominantly reside, as confirmed by confocal imaging. Although the TRPL setup does not have full confocality, due to the presence of the monochromator slits' aperture we can collect light coming from different planes and perform a quantitative quasi-Z-stack. This approach allowed us to identify differences in both intensity and decay dynamics within the sample out of plane direction, namely perpendicular to the myotubes plane. Notably, the signal intensity at time zero, proportional to the number of excited states generated, also provides information about the local concentration of Ziapin2. In the 3D hydrogel without cells, time zero intensity is identical at all depths. Since it is proportional to the local concentration of molecules, we can infer that the molecules are evenly distributed in the aqueous medium.

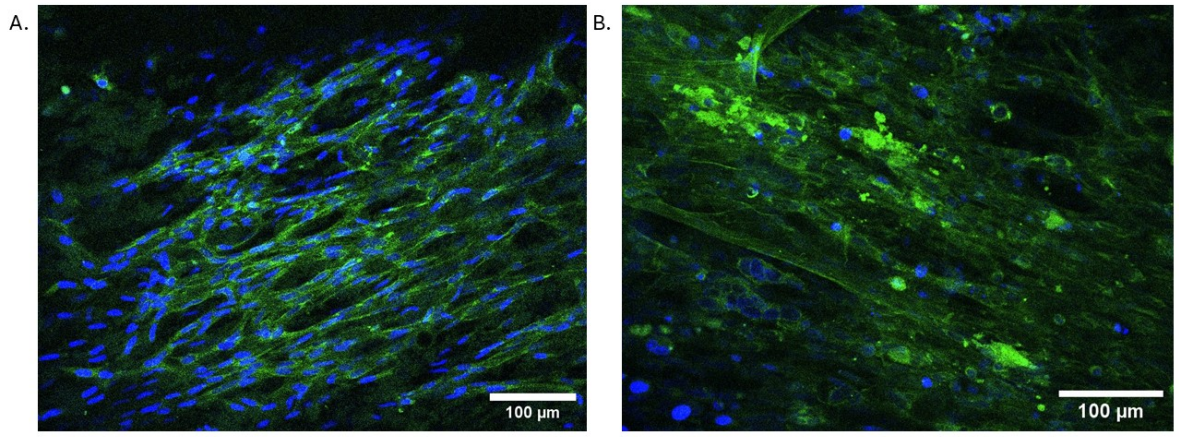

Figure 3. (**A**) Sample treated with Ziapin2, 25 µM. (**B**) Sample treated with Ziapin2, 50 µM. The nuclei of both images are stained with Hoechest (Blue), and Ziapin2 (Green).

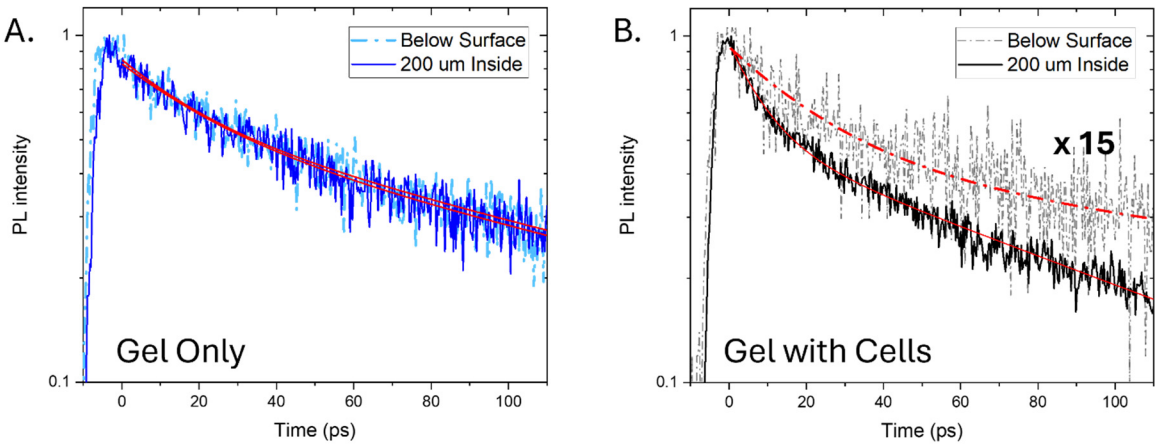

Figure 4. Time Resolved Photoluminescence traces of Ziapin2 normalized on the intensity maximum of the "200 um inside" decay (**A**) Comparison between decays taken in the Gel Only scaffold. (**B**) Comparison of the two curves taken in the Gel with Cells. The curve taken below surface is multiplied by 15 to match the other curves intensity at time zero.

Regarding decay dynamics, the results reported in Figure 4A are consistent with the one reported in water at both depths, having a radiative decay almost monexponential: fitting the curve with a biexponential to account such deviation from the single exponential, we obtained an average τ value of 105 ps, with the long component contributing (150 ps) more than 65% on the total decay (see Table S1 in SI for complete fitting parameter) and an initial faster (25 ps) component. Such almost monexponential behaviour and its average lifetime is coherent with reported data in water, slightly higher due to higher viscosity of the hydrogel compared to pure acqueous enviroment [18]. We can infer that Ziapin2 mostly does not undergo isomerization but emits PL from the locked trans isomer [19].

In contrast, in the hydrogel containing cells, a significant difference was observed between the surface and the bulk (see Figure 4B). First in terms of concentration: the PL intensity at time zero was almost 15 times higher

in the bulk, where cells predominantly reside, compared to the surface. This suggests that Ziapin2 penetrates the gel effectively and preferentially associates with cell membranes rather than remaining in the aqueous medium. Regardless of the gel's higher viscosity compared to water, the amphiphilic nature of Ziapin2 allows its accumulation in the myotubes rather than in the surrounding medium.

Second, in terms of dynamics, a faster (τ = 9.2 ps) component not measured in the pure hydrogel sample was detected in the bulk emission that was absent in the surface signal, with the relative weight being almost 50% of the total decay. Both τ and relative weight of this component are consistent with isomerization of Ziapin2 in cell membranes as previously reported (12 ps) [15]. The weak emission from the surface does not have such fast component and exhibited an average lifetime (100 ps) consistent with previous values in cell-free gel but with a slightly higher contribution of the fast component used to fit the gel decays (25 ps) [19]. It is worth noting that the highest contribution of the fast decay detected in the surface compared to gel only may be attributed to signal contributions from underlying layers, being the underlying bulk signal one order of magnitude higher than the surface one, rather than an actual different photophysical mechanism. This data further supports the conclusion that Ziapin2 is located within the cells' membrane and from the decay we can infer that the molecules isomerize as supported by their spectroscopic fingerprint.

We conclude that when the gel is exposed to Ziapin2, the molecule preferentially integrates into cell membranes escaping from surrounding hydrogel matrix, thus suggesting that an optical stimulus, would effectively trigger isomerization. We repeated the same measurements at different Ziapin2 concentrations, without observing any relevant difference. This indicates that the molecules portioning into cell membranes is concentration independent.

3.3. Contractions with Light

The experiments reported above demonstrate that (i) light fully diffuses within the 3D scaffold; (ii) Ziapin2 penetrates the gel and localize in the cell membrane; (iii) Ziapin2 photo isomerization is taking place in the 3D scaffold. These findings prompted us to attempt the optical stimulation of cell contraction within the 3D cell-seeded construct.

A sample incubated with Ziapin2 for one hour at a concentration of 50 µM was subjected to optical stimulation using 1 Hz light pulses. The effect of the stimulation was analyzed by recording videos (see representative Videos M1 and M2 in the Supplementary Information), captured using 4× and 20× objective lenses, respectively. Both recordings clearly demonstrate that light stimulation successfully induces contraction of the myotubes embedded within the hydrogel. From the video analysis, as described in the Materials and Methods section, we extracted the contraction profile along the x and y trajectories of a selected region of the 3D construct, as well as the resulting displacement. As shown in Figure 5 and in Figures S6–S8 of the Supplementary Information, the construct contraction profile (blue line) begins with the light pulse and follows the 1 Hz photostimulation (orange line). Moreover, Figure 5B shows that the displacement distribution in both x and y directions is homogeneously distributed. These results confirm the functional integration of Ziapin2 into cellular architecture and support its potential as a photostimulatory agent also in more complex systems as 3D hydrogels. This finding paves the way for future developments in the field of light-controlled actuation in biohybrid systems.

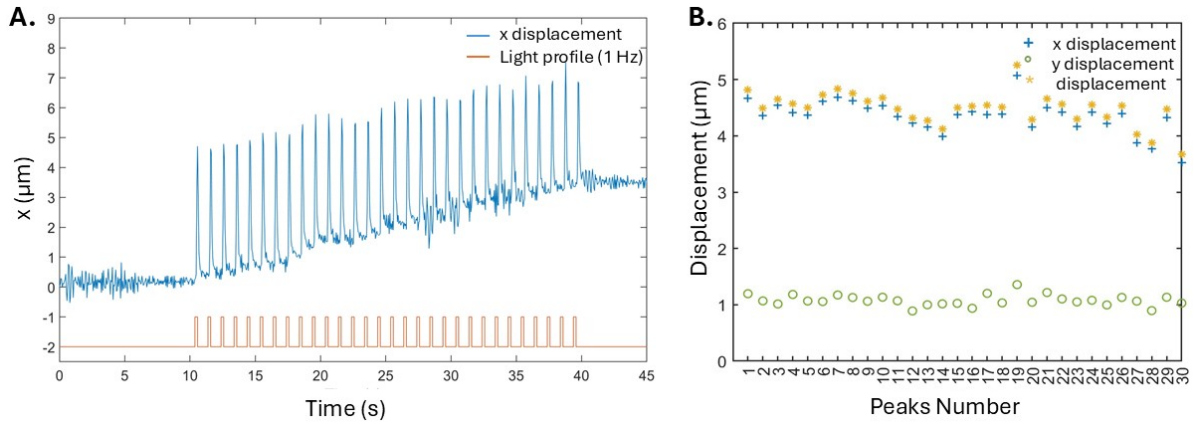

Figure 5. (**A**) Contraction profile of the selected region along the x trajectory (blue line) and the 1 Hz stimulation protocol (orange line). (**B**) Displacement distribution in the x and y directions, and the resulting displacement vector for each peak.

4. Conclusions

The development of three-dimensional (3D) artificial cell networks is attracting growing interest, as these systems more closely mimic the structural and functional complexity of natural tissues. This is particularly relevant for hybrid actuators, integrating both abiotic and biotic components, where transitioning from traditional two-dimensional (2D) designs to 3D architectures results in improved performance, including enhanced contractile strength and responsiveness.

In this study, we present a detailed characterization of a 3D construct composed of a hydrogel volume seeded with C2C12 skeletal muscle cells, that could be used for realizing photoresponsive biohybrid actuators. Our aim was to assess the key physical of the system, while also identifying potential failure modes that could compromise functionality.

To achieve light-induced actuation, we employed Ziapin2, a recently developed molecular phototransducer that functions effectively when embedded in the cell membrane. We investigated several aspects critical to system performance: the penetration of light through the hydrogel, the extent of cell colonization within the 3D matrix and the cell differentiation, the diffusion and localization of Ziapin2, and the ability to induce contraction through light stimulation.

The results are encouraging. Contrary to initial concerns, light was found to penetrate the hydrogel fully, and Ziapin2 efficiently reached the cell membranes rather than becoming trapped in the gel matrix. Most importantly, light-induced contraction of the 3D cell-laden construct was successfully demonstrated, confirming the feasibility of the approach. Future improvements will focus on increasing the density of contractile cells within the construct to enhance mechanical output and on optimizing conditions for long-term cell viability. As this system remains biologically active, maintaining appropriate nutrient supply and environmental homeostasis will be essential.

Overall, this work represents a promising step toward the realization of functional 3D photoresponsive biohybrid actuators, with potential applications in soft robotics and tissue-engineered systems.

Supplementary Materials

The additional data and information can be downloaded at: https://media.sciltp.com/articles/others/2512081011011769/PS-25100140S-SM-R1.zip. Figure S1: Procedure for Ink production. Figure S2: Printed Mask. Table T1: TRPL Table Fitting. Figure S3: Snapshots from the contraction videos. Figure S4: Extended Confocal Images. Figure S5: TRPL different concentration. Figure S6–S8: 3D constructs contraction traces and displacement distribution. Movies M1 and M2: Contraction Movies.

Author Contributions

A.P.: conceptualization, methodology, investigation, data curation, software, validation, formal analysis, writing—original draft; I.V.: conceptualization, methodology, investigation, data curation, formal analysis, writing—original draft; G.S.: data curation, formal analysis, visualization, writing—review and editing; S.S.: investigation, methodology; L.A.: investigation, visualization; P.M.: Resources; G.M.P: supervision, validation, writing—review & editing; C.B.: Funding acquisition; C.D.: supervision, validation, writing—review & editing; G.L.: conceptualization, methodology, founding acquisition, project administration, supervision, writing—review and editing. All authors have read and agreed to the published version of the manuscript.

Funding

A.P. and G.L. aknowledge Fondo Italiano per la Scienza project (ID FIS00001244). G.M.P. thanks the European Union for financial support (ERC, EOS, 101115925).

Institutional Review Board Statement

Not applicable.

Informed Consent Statement

Not applicable.

Data Availability Statement

The authors confirm that the data supporting the findings of this study are available within the article.

Conflicts of Interest

The authors declare no conflict of interest.

Use of AI and AI-Assisted Technologies

No AI tools were utilized for this paper.

References

1. Pfeffer, M.E.; DiFrancesco, M.L.; Marchesi, A.; et al. Nanoactuator for Neuronal Optoporation. *ACS Nano* **2024**, *18*, 12427–12452. https://doi.org/10.1021/acsnano.4c01672.
2. Lee, Y.; Song, W.J.; Sun, J.-Y. Hydrogel Soft Robotics. *Mater. Today Phys.* **2020**, *15*, 100258. https://doi.org/10.1016/j.mtphys.2020.100258.
3. Wang, C.; Zhang, Z.; Wang, J.; et al. Biohybrid Materials: Structure Design and Biomedical Applications. *Mater. Today Bio.* **2022**, *16*, 100352. https://doi.org/10.1016/j.mtbio.2022.100352.
4. Yan, B. Actuators for Implantable Devices: A Broad View. *Micromachines* **2022**, *13*, 1756. https://doi.org/10.3390/mi13101756.
5. Sun, L.; Yu, Y.; Chen, Z.; et al. Biohybrid Robotics with Living Cell Actuation. *Chem. Soc. Rev.* **2020**, *49*, 4043–4069. https://doi.org/10.1039/D0CS00120A.
6. Webster-Wood, V.A.; Guix, M.; Xu, N.W.; et al. Biohybrid Robots: Recent Progress, Challenges, and Perspectives. *Bioinspir. Biomim.* **2022**, *18*, 015001. https://doi.org/10.1088/1748-3190/ac9c3b.
7. Revete, A.; Aparicio, A.; Cisterna, B.A.; et al. Advancements in the Use of Hydrogels for Regenerative Medicine: Properties and Biomedical Applications. *Int. J. Biomater.* **2022**, *2022*, 3606765. https://doi.org/10.1155/2022/3606765.
8. Sun, W.; Schaffer, S.; Dai, K.; et al. 3D Printing Hydrogel-Based Soft and Biohybrid Actuators: A Mini-Review on Fabrication Techniques, Applications, and Challenges. *Front. Robot. AI* **2021**, *8*, 673533. https://doi.org/10.3389/frobt.2021.673533.
9. Balint, R.; Cassidy, N.J.; Cartmell, S.H. Electrical Stimulation: A Novel Tool for Tissue Engineering. *Tissue Eng. Part B Rev.* **2013**, *19*, 48–57. https://doi.org/10.1089/ten.teb.2012.0183.
10. Antognazza, M.R.; Martino, N.; Ghezzi, D.; et al. Shedding Light on Living Cells. *Adv. Mater.* **2015**, *27*, 7662–7669. https://doi.org/10.1002/adma.201403513.
11. Vurro, V.; Venturino, I.; Lanzani, G. A Perspective on the Use of Light as a Driving Element for Bio-Hybrid Actuation. *Appl. Phys. Lett.* **2022**, *120*, 080502.
12. DiFrancesco, M.L.; Lodola, F.; Colombo, E.; et al. Neuronal Firing Modulation by a Membrane-Targeted Photoswitch. *Nat. Nanotechnol.* **2020**, *15*, 296–306. https://doi.org/10.1038/s41565-019-0632-6.
13. Venturino, I.; Vurro, V.; Bonfadini, S.; et al. Skeletal Muscle Cells Opto-Stimulation by Intramembrane Molecular Transducers. *Commun. Biol.* **2023**, *6*, 1148. https://doi.org/10.1038/s42003-023-05538-y.
14. Florindi, C.; Simoncini, G.; Lanzani, G.; et al. Shining Light in a Heartbeat: Controlling Cardiac Bioelectricity with Membrane-Targeted Photoswitches. *Appl. Phys. Lett.* **2025**, *126*, 230501. https://doi.org/10.1063/5.0270696.
15. de Souza-Guerreiro, T.C.; Bondelli, G.; Grobas, I.; et al. Membrane Targeted Azobenzene Drives Optical Modulation of Bacterial Membrane Potential. *Adv. Sci.* **2023**, *10*, 2205007. https://doi.org/10.1002/advs.202205007.
16. Moschetta, M.; Vurro, V.; Sesti, V.; et al. Modulation of Mechanosensitive Potassium Channels by a Membrane-Targeted Nongenetic Photoswitch. *J. Phys. Chem. B* **2023**, *127*, 8869–8878. https://doi.org/10.1021/acs.jpcb.3c04551.
17. Tummala, G.K.; Felde, N.; Gustafsson, S.; et al. Light Scattering in Poly(Vinyl Alcohol) Hydrogels Reinforced with Nanocellulose for Ophthalmic Use. *Opt. Mater. Express OME* **2017**, *7*, 2824–2837. https://doi.org/10.1364/OME.7.002824.
18. Magni, A.; Bondelli, G.; Paterno, G.M.; et al. Azobenzene Photoisomerization Probes Cell Membrane Nanoviscosity. *Phys. Chem. Chem. Phys.* **2022**, *24*, 8716–8723. https://doi.org/10.1039/D1CP05881A.
19. Paternò, G.M.; Colombo, E.; Vurro, V.; et al. Membrane Environment Enables Ultrafast Isomerization of Amphiphilic Azobenzene. *Adv. Sci.* **2020**, *7*, 1903241. https://doi.org/10.1002/advs.201903241.